 doi:10.20944/preprints202209.0072.v1

*Article*

# Modeling the Regional Effects of Climate Change on Future Urban Ozone Air Quality in Tehran, Iran

**Ehsan Mosadegh [1,*], Iman Babaeian [2], Khosro Ashrafi [3], and Majid Shafiepour Motlagh [4]**

[1] Atmospheric Sciences Graduate Program, University of Nevada, Reno, NV 89557, USA.; emosadegh@nevada.unr.edu
[2] Climate Research Institute, Atmospheric Science and Meteorological Research Center, Mashhad, Iran; i.babaeian@gmail.com
[3] Department of Environmental Engineering, Graduate Faculty of Environment, University of Tehran, Tehran, Iran.; khashrafi@ut.ac.ir
[4] Department of Environmental Engineering, Graduate Faculty of Environment, University of Tehran, Tehran, Iran.; shafiepourm@yahoo.com
* Correspondence: Corresponding author: emosadegh@nevada.unr.edu

**Abstract:** We developed an artificial neural network as an air quality model and estimated the scope of the impact of climate change on future (until 2064) summertime trends of hourly Ozone (O3) concentrations at an urban air quality station in Tehran, Iran. Our developed scenarios assume that present-time emissions conditions of O3 precursors will remain constant in the future. Therefore, only the impact of climate change on future O3 concentrations is investigated in this study. GCM projections indicate more favorable climate conditions for O3 formation over the study area in the future: the surface temperature increases over all months of the year, solar radiation increases, and precipitation decreases in future summers, and summertime daily maximum temperature increases about 1.2 °C to 3 °C until 2064. In the scenario based on present-time O3 conditions in 2012 summer without any exceedances, the summertime exceedance days of 8-hr O3 standard are projected to increase in the future by about 4.2 days in the short term and about 12.3 days in the mid-term. Similarly, in the scenario based on present-time O3 conditions in 2010 summer with 58 days of exceedance from 8-hr O3 standard, exceedances are projected to increase about 4.5 days in the short term and about 14.1 days in the mid-term. Moreover, the number of Unhealthy and Very Unhealthy days in 8-hr AQI is also projected to increase based on pollution scenarios of both summers.

**Keywords:** Ozone; climate change; air quality modeling; artificial neural networks; statistical downscaling; Tehran

## 1. Introduction

Intergovernmental Panel on Climate Change (IPCC) projections indicate that climate change may influence future air quality and the magnitude of the impact varies from one region to another (IPCC, 2007). One of the challenges associated with air quality studies is to quantify this influence on air pollutants such as Ozone (O3) and PM which are sensitive to climate changes (Jacob and Winner, 2009). Surface O3, which is one of the most important air pollutants, degrades public health by damaging the respiratory system. It is a secondary pollutant which means it is not emitted from a particular source but is produced through complex photochemical reactions among its biogenic and anthropogenic precursors such as NOx, NMVOC, CO and CH4 in the presence of high temperature and abundant sunlight (Jacob and Winner, 2009; Seinfeld and Pandis, 2006; Steiner et al., 2006). NOx and CO come from combustion sources, but NMVOC and CH4 have several natural and anthropogenic sources (Guenther et al., 2000; Sillman, 1999). Therefore, due to its photochemical nature, O3 concentrations generally peak during the summer season when meteorological conditions are often favorable for its formation. O3 has an atmospheric lifetime of about few days in the boundary layer with global sinks of dry deposition and

 doi:10.20944/preprints202209.0072.v1



photolysis in the presence of water vapor (Jacob and Winner, 2009). This oxidant pollutant irritates pulmonary system and decreases lung function. O3 is believed to be associated with premature mortality and exposure to its elevated concentrations irritates people who have respiratory diseases such as asthma and pneumonia (Bell et al., 2007; Ebi and McGregor, 2008; Gryparis et al., 2004).

Meteorological parameters play an important role in O3 production. temperature, solar radiation, atmospheric moisture, wind, mixing height, precipitation and cloud cover are identified to be correlated with O3 (Camalier et al., 2007; Dawson et al., 2007; Leibensperger et al., 2008; Mott et al., 2005; Ordóñez et al., 2005). Among these variables, O3 is highly sensitive to temperature (Cox and Chu, 1996; Dawson et al., 2007; Sillman and Samson, 1995). The emission of biogenic VOCs which is a temperature dependent process can produce a considerable amount of O3 in high temperatures (Fuentes et al., 2000; Lee and Wang, 2006; Narumi et al., 2009). However, in addition to temperature, solar radiation is also necessary for the photochemical process of O3 formation in the atmosphere. The correlation between these variables is significant especially in summers when high radiation and temperature result in summertime high O3 concentrations (Ordóñez et al., 2005).

There are two major sources of uncertainty in projections of the impact of climate change on future O3 formation: estimating the future emissions of O3 precursors and projecting the meteorological factors that strongly influence air quality (Dawson et al., 2007; Ebi and McGregor, 2008; Steiner et al., 2006). Studies that have investigated the influence of projected changes in climate variables on future O3 concentrations by assuming no changes in the emissions of O3 precursors (Dawson et al., 2009; Liao et al., 2006; Murazaki and Hess, 2006; Racherla and Adams, 2006) indicate that the projected changes in climate variables are expected to increase future O3 concentration levels over and near polluted regions. The extent of this increase, although varying in different regions, highlights the role of future meteorological conditions in O3 production and suggests that future meteorological parameters will shift toward more favorable conditions for O3 formation (Murazaki and Hess, 2006). We can perform sensitivity studies to evaluate how much changes in future emissions and climate can affect future O3 production (Dawson et al., 2007; Millstein and Harley, 2009; Orru et al., 2013; Steiner et al., 2006). Steiner et al. (2006) found that combined climate perturbations (such as increases in temperature and water vapor together with temperature-induced increase in biogenic VOC emissions) yield to increased peak O3 concentrations. Their results indicate that sensitivity of O3 to climate change is regionally different and the sensitive regions may experience more exceedances despite the present emission reduction policies and therefore additional control on pollution emission reductions will be needed.

To study the impact of climate change on future O3 air quality both statistical and dynamical approaches can be used (Wise, 2009). Dynamical models have distinct advantages over statistical approaches. However, some benefits of statistical models cannot be ignored. Statistical models are widely known for their computationally inexpensive cost and capability of rapid climate change impact assessment by employing various climate models and scenarios. For instance, Varotsos et al. (2013) developed a statistical model between daily maximum temperature and hourly O3 concentrations over Europe for the periods of 2021–2050 and 2071–2100 to investigate the impact of climate change on the number of days with O3 exceedances of 60 ppb. They observed that higher daily temperatures due to climate change will result in considerable increases in O3 exceedance days in the future. Also, one can use a statistical technique to downscale the GCM data and to model the relationship between observed O3 concentrations and meteorological variables to project the potential impact of future meteorology on O3 exceedances of 84 ppb (Holloway et al., 2008). Due to the coarse spatial resolution of GCM models, some of the small-scale but important processes are not captured in GCM simulations (Holloway et al., 2008). Also, dynamical models that are developed based on current physical parameterizations may not be able to perfectly simulate future changes in climate variables. For instance, Lynn et al. (Lynn et al., 2004) showed that in order for climate change simulations

 doi:10.20944/preprints202209.0072.v1



to provide a realistic estimate of changes in temperature, models should correctly simulate the diurnal precipitation over the study region.

Climate change projections (IPCC, 2021) indicate that projected changes in climate variables such as precipitation and temperature (Mosadegh and Babaeian, 2022a) will impact different components of the climate system with different magnitude and confidence and in all regions of the world (Mejia et al., 2018; Mosadegh et al., 2018; Mosadegh and Nolin, 2020). Several studies have addressed the issue of air quality in Tehran (Arhami et al., 2013; Ashrafi, 2012; Atash, 2007; Hosseinpoor et al., 2005; Hoveidi et al., 2013). However, a few studies have investigated uncertainty of those climate projections over the 21st century (Mosadegh and Babaeian, 2022b), and the extent that the projected climate variables can affect air pollution of Tehran region (Mosadegh, 2013). The present study is the first attempt to evaluate the regional impact of climate change on air quality in Iran. The aim of this study is to develop and apply a statistical approach to investigate the impact of climate change on future O3 air quality on a local scale in an urban environment. In this study, an artificial neural network was used as a predictive tool which is capable of capturing nonlinearities in atmospheric processes such as O3 formations (Comrie, 1997; Gardner and Dorling, 1998). The projected O3 concentrations were analyzed based on exceedances of O3 air quality standards and health-related air quality indices. To simplify the impact assessment process, only climate variables of solar radiation and temperature together with pollutants of NO and NO2 were considered in the simulation process. In this study, the relationship between O3 and local meteorology was partially accounted by considering hourly temperature and solar radiation values in the development process of the Artificial Neural Network as the air quality forecast model (AQFM). Emissions of O3 precursors were also taken into account but were considered constant based on current conditions. Therefore, only the impact of climate change was investigated on future O3 concentrations in Tehran.

## 2. Methodology

This study is comprised of a few major steps: in the first step, we downscaled GCM data under different emission scenarios. In the second step, we downscaled the daily climate variables from previous step from daily scale to sub-daily (hourly) scale. In the third step, we developed input scenarios and developed an artificial neural network as the AQFM, and in the final step we assessed the impact of climate change on future O3 air quality. These steps are described in detail in next sections.

### *2.1. Case study and data*

Tehran, the capital of Iran, is the largest city in Iran with the population of more than 10 million people and with the area of approximately 570 square kilometers. Tehran is surrounded by mountains to the north and the east, and the wind directions are from the west and the south. Tehran suffers from serious air pollution problems. Motor vehicles are considered as one of the major sources of air pollution in Tehran metropolitan area due to their high emission of major pollutants such as CO, PM10 and NO2 (Halek et al., 2004). In Tehran, air pollution concentrations are monitored by Air Quality Control Company (AQCC) and Department of Environment (DOE) in several air quality stations. In this study, the air quality data were obtained from the AQCC Golbarg air quality monitoring station east of Tehran at 35° 43′ N and 51° 30′ E. In order to develop and evaluate our AQFM (ANN), hourly monitored Nitrogen Monoxide (NO), Nitrogen Dioxide (NO2), O3, Solar Radiation (SR) and Temperature (T) collected at this station during 2009–2012 were used. Meteorological data were obtained from the Dushan Tappeh station, the nearest synoptic station located at 35° 42′ N and 51° 20′ E with the height of 1209 m above sea level. From this station daily minimum temperature, daily maximum temperature, total precipitation and total sunshine hours during 1972–2009 (baseline period) were used to calibrate the LARS-WG statistical downscaling model.

 doi:10.20944/preprints202209.0072.v1



*2.2. Statistical downscaling with LARS-WG*

Different dynamic and statistical models have been developed to downscale the GCM outputs (Wilby et al., 2004). Stochastic weather generators (WG) are one of the statistical downscaling tools which generate daily time series of climate variables (Semenov, 2007; Wilks and Wilby, 1999). In this study, Long Ashton Research Stochastic Weather Generator (LARS-WG) is employed to downscale the GCM projections and to estimate future changes in temperatures, solar radiation and precipitation over the study area. LARS-WG (Semenov and Barrow, 2002) is a stochastic weather generator (WG). The model takes observed daily minimum temperature, maximum temperature, total precipitation and total sunshine hours as its inputs and generates synthetic daily time series at any local scale. LARS-WG generates local-scale climate change scenarios for a given site by adjusting baseline parameters, calculated from baseline observed weather at the site, with projected GCM $\Delta$-changes, calculated based on an SRES emission scenario and a future climate period, for each climatic variable (Semenov and Stratonovitch, 2010). More details about the application of LARS-WG model can be found in Mosadegh and Babaeian (2022a, 2022b). The ability of the LARS-WG to simulate the baseline climate variables at the given site was evaluated by calculating the Pierson correlation coefficient (R) and error indices such as mean bias error (MBE), mean absolute error (MAE) and root mean square error (RMSE).

*2.3. The AQFM*

With recent advances in deep learning for pattern recognition, performance of these networks for the task of prediction in different fields of environmental science has progressed even with small amount of training data (Alibak et al., 2022; Nejatishahidin et al., 2022). Application of artificial neural networks (ANN), especially multilayer perceptions (MLP) in the field of air quality has been evaluated in many studies (Chaloulakou et al., 2003; Comrie, 1997; Niska et al., 2004; Schlink et al., 2003; Sousa et al., 2007). Application of the neural networks in forecasting O3 concentrations has been compared with other statistical tools such as multivariate linear regression models, and the results indicate that the ANNs especially the MLP neural network has a better performance over other techniques in modeling the O3 nonlinear associations (Gardner and Dorling, 1998). Furthermore, it can model highly nonlinear processes by its activation and transfer functions in the hidden layers (Rahnama and Noury, 2008). These features make MLP a suitable tool for modeling complex, nonlinear phenomena such as O3 formation in the atmosphere.

In this study, a four-layer MLP with a 4-10-10-1 (4 inputs with 1 output) network structure was used. Tangent sigmoid transfer functions (*tansig*) were used in the hidden layers, but a linear transfer function (*purlin*) was used in the output layer. For training the network, the Levenberg-Marquardt back-propagation learning rule (*trainlm*) was used due to its fast speed and accuracy in training the system (Beale et al., 2012).

To determine the model inputs, we considered effective variables in O3 production (Ordóñez et al., 2005) and the limited number of available monitored variables at the Golbarg air quality control station. Finally, we selected Nitrogen Oxide (NO), Nitrogen Dioxide (NO2) and O3 as the air quality variables and temperature (T) and Solar Radiation (SR) as climate variables to develop the AQFM. It is noteworthy that the selected variables were monitored at *Golbarg* air quality monitoring stations during the summers (June, July and August, hereafter JJA) of 2009–2012.

To develop the AQFM, data samples were initially investigated, and defective data samples were excluded from the training data set. The selection of the datasets for developing the forecast model was limited to the 8 am to 7 pm interval which is the most effective period of O3 production during the day. Finally, about 4000 hourly data samples were obtained for the summers (JJA) of 2009 to 2012 to develop the forecast model. The training data set was shuffled randomly to scatter maximum and minimum values evenly over the entire training data set. Then, data samples were divided to three subsets of training, test

 doi:10.20944/preprints202209.0072.v1



and validation sets with 60-20-20 percent of the data set, respectively. Since the input and target variables did not have a uniform range of values, a normalization method was used to scale the input variables to have a certain range. In this study, normalization of the variables was performed by the $mapminmax$ function in MATLAB to scale the data to the range [-1, 1] before fitting data to the main network. In order to achieve the best relationship between input variables and output target (O3), different network architectures were examined. Finally, the network structure with the smaller error and the higher correlation was selected as the optimal predictive model.

In order to evaluate the performance of the AQFM, we calculated the correlation coefficient (R) and statistical parameters such as mean bias error (MBE), mean absolute error (MAE) and root mean square error (RMSE). After ensuring the accuracy of the simulations of the developed model to reproduce hourly O3 concentrations with regard to high correlation coefficient and low error indices compared to similar studies (Arhami et al., 2013; Comrie, 1997; Sousa et al., 2007), performance of the forecast model was assessed based on two performance indices. In this study, the prediction of exceedances of desired O3 air quality concentration thresholds were more important than predicting the exact O3 concentration values. Therefore, we developed 2 metrics to define capturing the occasions in which the O3 concentrations exceed a desired O3 air quality threshold. The 2 performance indices of PI1 and PI2 are described bellow:

PI1: The percentage of correctly identified occasions in which O3 concentrations exceeded a desired threshold.

PI2: The percentage of incorrectly identified occasions.

PI1 indicates the forecasting accuracy of the predicting model at each concentration threshold. This index represents the percentage of the cases that both monitored values and corresponding simulated values exceed a desired concentration threshold and consequently the model is successful in predicting the exceedance. PI2 indicates the overestimation error of the model at each concentration threshold. This index represents the percentage of cases that observations do not exceed the desired concentration threshold, but the model incorrectly indicates that the corresponding simulated values exceed the desired threshold.

In order to assess the accuracy of the AQFM in simulating the exceedances, several important O3 concentration thresholds were considered from various EPA ozone air quality standards and indices. The test data set of the model was examined to assess the accuracy of the model in predicting the exceedances. The investigated EPA thresholds are significant levels of O3 concentrations in 1-hr O3 air quality standard and air quality index (AQI). Exceeding these threshold concentrations results in occurrence of an *Unhealthy* day (O3 concentration above 125 ppb) and a *Very Unhealthy* day (O3 concentrations above 205 ppb) from AQI perspective, and occurrence of a polluted day (O3 concentrations above 120 ppb) from 1-hr O3 standard perspective. In addition to mentioned thresholds, accuracy of the forecast model in predicting exceedances of other concentration thresholds (25 ppb and 45 ppb) were also evaluated to enable us to compare the performance of the developed model with similar studies.

### *2.4. Temporal (sub-daily) downscaling*

LARS-WG generates minimum and maximum temperature values for each single day. Solar radiation is also generated in $Mj/m^2.day$ and represents the total solar radiation reaching the earth surface in a single day. However, the AQFM was developed based on hourly (sub-daily) variables and received hourly temperature and radiation values as its inputs. For the LARS-WG output to match the AQFM inputs in hourly (sub-daily) scale, we developed the diurnal distribution equations of the temperature and solar radiation at the given site to calculate diurnal distribution of these variables.

#### 2.4.1. Diurnal patterns of future temperature

Preprints (www.preprints.org) | NOT PEER-REVIEWED | Posted: 6 September 2022 doi:10.20944/preprints202209.0072.v1



Accurately estimating the diurnal patterns of temperature in the future is important in assessing the impact of climate change on peak O3 concentration levels (Millstein and Harley, 2009). To obtain future hourly temperatures, the diurnal pattern of future temperature was anticipated by developing a sinusoidal equation as a function of time of day (Ephrath et al., 1996)

$$T_a = T_{min} + (T_{max} - T_{min}) * S_t \quad (1)$$

where $T_a$ is the air temperature during daytime, $T_{min}$ and $T_{max}$ are the minimum and maximum air temperature respectively and $S_t$ is a function of time $t$, ranging between 0 and 1, which is defined as

$$S_t = sin(\pi \frac{t - LSH + \frac{DL}{2}}{DL + 2P}) \quad (2)$$

where $DL$ is the day length, $LSH$ is the local time of maximum solar height during the day and $P$ is the delay in the maximum air temperature with respect to the time of maximum solar height at the site.

To estimate the air temperature at night, a declining exponential equation was used (Ephrath et al., 1996)

$$T_a = A + Bexp(-\frac{t}{\tau}) \quad (3)$$

which was developed to

$$T_a = \frac{T_{min(J+1)} - T_s exp(-\frac{\alpha}{\tau} + (T_s - T_{min}(J+1)))exp(\frac{t_a - t_s}{\tau})}{1 - exp(-\frac{\alpha}{\tau})} \quad (4)$$

where $\tau$ is a time coefficient which was considered 4; $t_s$ and $t_a$ are the time of sunset and the current time, respectively, and $\alpha$ is the night length ($\alpha$ = 24 - DL). Values of $DL$, $LSH$ and $P$ were extracted from temperature and solar radiation graphs which were obtained by studying the variability of parameters during the observation period in the station under study. After inserting these parameters in the equations and by using the daily minimum and maximum temperature from LARS-WG outputs, hourly temperature values were calculated.

2.4.2. Diurnal patterns of future radiation

LARS-WG generates its solar radiation output in $Mj/m^2.day$ as the total daily radiation received by the earth surface in a single day. However, the AQFM accepts hourly values in $W/m^2$ as its radiation input. To match the scale of LARS-WG radiation output to the scale of the inputs to the air quality model, some equations were developed to estimate the diurnal patterns of solar radiation. The diurnal radiation curve was calculated by obtaining parameters such as daily total radiation ($R_g$), day length ($DL$) and solar elevation ($sin\beta$), computed from the latitude of the site ($L$, radians), the solar declination angle ($\delta$, radians) and time of the day ($t_a$). To compute the sine of the solar elevation ($sin\beta$) some intermediate parameters were needed: $SD$, the seasonal offset of the sine of the solar height

$$SD = sin(L) * sin(\delta) \quad (5)$$

and $CD$, the amplitude of the sine of the solar height

$$CD = cos(L) * cos(\delta) \quad (6)$$

The sine of the solar elevation, $sin\beta$, is calculated as

$$sin\beta = SD + CD * cos(\pi \frac{t_a - LSH}{12}) \quad (7)$$

where $t_a$ is the current time and $LSH$ is the time of maximum solar height. Instantaneous radiation ($R_g$) is computed as

$$R_g = R_g(tot) * sin\beta * \frac{1 + C * sin\beta}{DSBE * 3600} \quad (8)$$

where $DSBE$ is the daily integral of $sin\beta(1 + sin\beta)$ from sunrise to sunset, calculated as

$$DSBE = arccos(-\frac{SD}{CD})\frac{24}{\pi}(SD + C * SD^2 + \frac{C * CD^2}{2}) + 12 * CD * (2 + 3C * SD) * \frac{\sqrt{1 - \frac{SD^2}{CD}}}{\pi} \quad (9)$$

Preprints (www.preprints.org) | NOT PEER-REVIEWED | Posted: 6 September 2022 doi:10.20944/preprints202209.0072.v1



The parameter $C$ (Eqs. (8) and (9)) is a constant meteorological variable, and is considered equal to 0.4 (Spitters et al., 1986). In order to calculate $SD$ and $CD$, a parameter called $\delta$ is used to represent the solar declination angle. For obtaining hourly values of solar declination angle, proposed equations by Jacobson (Jacobson, 2005) were used

$$\delta = arcsin(sin\varepsilon_{ob} * sin\lambda_{ec}) \quad (10)$$

where $\lambda_{ec}$ represents the ecliptic longitude of the Sun and $\varepsilon_{ob}$ represents the obliquity of the ecliptic. The ecliptic is the mean plane of the orbit of the Earth when it moves around the Sun. The obliquity of the ecliptic represents the angle between the plane of the Earth's Equator and the plane of the ecliptic, which is approximated as

$$\varepsilon_{ob} = 23°.439 - 0°.0000004N_{JD} \quad (11)$$

where

$$N_{JD} = 364.5 + (Y - 2001) * 365 + D_L + D_J \quad (12)$$

$$D_L = \{\left|\frac{(Y-2001)}{4}\right| \quad Y \geq 2001 \ or \ \left|\frac{(Y-2000)}{4} - 1\right| \quad Y < 2001\} \quad (13)$$

where $N_{JD}$ represents the number of days from the beginning of Julian year 2000. In Eqs. (12) and (13), $Y$ is the current year, $D_L$ is the number of leap days since or before the year 2000 and $D_J$ is the Julian day of the year, which varies from 1 on $1^{st}$ of January to 365 (for non-leap years) or 366 (for leap years) on $31^{st}$ of December. Leap years occur every year evenly divisible by 4. The ecliptic longitude of the Sun is approximately

$$\lambda_{ec} = L_M + 1°.915sin(g_M) + 0°.020sin(2g_M) \quad (14)$$

where

$$L_M = 280°.460 + 0°.9856474N_{JD} \quad (15)$$

$$g_M = 357°.528 + 0°.9856003N_{JD} \quad (16)$$

$L_M$ and $g_M$ are the mean longitude of the Sun and the mean anomaly of the Sun, respectively. The mean anomaly of the Sun is the angular distance, as seen by the Sun, of the Earth from its perihelion, which is the point in the Earth's orbit at which the Earth is closest to the Sun by assuming that the Earth's orbit is perfectly circular, and the Earth is moving at a constant speed.

### *2.5. Development of input scenarios to the AQFM*

Estimating the future O3 concentrations under climate change required estimating the future pollution emissions together with climate conditions for the desired periods. These combinations served as inputs to our AQFM (ANN). Therefore, a combination of some pollution and climate conditions were developed as input scenarios to the AQFM to represent some probable future conditions.

#### 2.5.1. Air quality scenarios

Estimating future O3 air quality conditions involve several assumptions and uncertainties (Ebi and McGregor, 2008). Future O3 production is dependent on emissions of its future biogenic and anthropogenic precursors such as NOx and VOCs. Estimating future emissions of these precursors depend on key factors such as population growth, energy consumption, technology advancement and socio-economic developments which further involves considering limitations and uncertainties for the distant future (Webster et al., 2002). Furthermore, in this study, the AQFM (ANN) was trained by hourly resolution. Due to present limitations and uncertainties, we decided to limit our study to only the impact of climate change alone on future O3 air quality. Therefore, current pollution conditions were assumed to remain constant in the future based on hourly monitored NO and NO2 concentrations in the summers of 2010 and 2012, which were considered as representations of highly polluted and unpolluted summertime conditions, respectively.

#### 2.5.2. Climate change scenarios

Based on considered assumptions and limitations in the previous section we limited our study to only the effect of climate change on current pollution conditions. In this study, we used three IPCC greenhouse gas emission scenarios to simulate future climate:

Preprints (www.preprints.org) | NOT PEER-REVIEWED | Posted: 6 September 2022 doi:10.20944/preprints202209.0072.v1



A1B, A2, and B1, which their emissions are equivalent to RCP4.5, RCP8.5, and RCP2.6, respectively. In this study, climate projections from HadCM3 AOGCM were used. This GCM is a coupled atmospheric-oceanic model which has been used and suggested in several previous studies (Hessami et al., 2008; Holloway et al., 2008; Lioubimtseva and Henebry, 2009; Zarghami et al., 2011). This model simulates the global climate with 19 levels in its atmospheric component with a horizontal resolution of 2.5° by 3.75° degrees (latitude by longitude) and 20 levels in its oceanic component with a horizontal resolution of 1.25° by 1.25° degrees.

## 3. Results and discussion

### *3.1. Verification of LARS-WG*

To verify the downscaled results, the ability of LARS-WG to simulate the baseline climate (1972–2009) was evaluated by coefficient of determination ($R^2$), statistical tests such as t-test and K-S test, and statistical parameters such as RMSE, MAE and MBE. Table 1 indicates the calculated statistical parameters for the simulated monthly means of the climatic variables by LARS-WG in the baseline period. Except for precipitation that has the highest simulation error, other error indices are relatively low for all variables which demonstrate the acceptable agreement between the observed and simulated monthly means in the baseline period in the study area.

**Table 1.** Calculated statistical parameters for the simulated monthly means of the variables by LARS-WG in the baseline period at the Dushan Tappeh station (1972–2009).

| **Climatic variables** | **Error Indices** | | |
|---|---|---|---|
| | MBE | MAE | RMSE |
| Minimum Temperature | -0.03 | 0.12 | 0.15 |
| Maximum Temperature | 0.08 | 0.19 | 0.23 |
| Solar Radiation | 0.12 | 0.28 | 0.33 |
| Precipitation | 2.9 | -20.2 | -24.5 |

### *3.2. Regional changes in climate*

Figure 1 illustrates the HadCM3 projected absolute changes in surface minimum and maximum temperature for Dushan Tappeh station under A2, A1B and B1 emission scenarios. Projections were obtained for the future periods of 2015–2039 (short term) and 2040–2064 (mid-term) relative to the baseline period (1972–2009). Long term monthly means of observed minimum and maximum temperatures in the baseline period are also illustrated on this Figure to provide an estimate of the future annual temperature patterns in the study area under climate change.

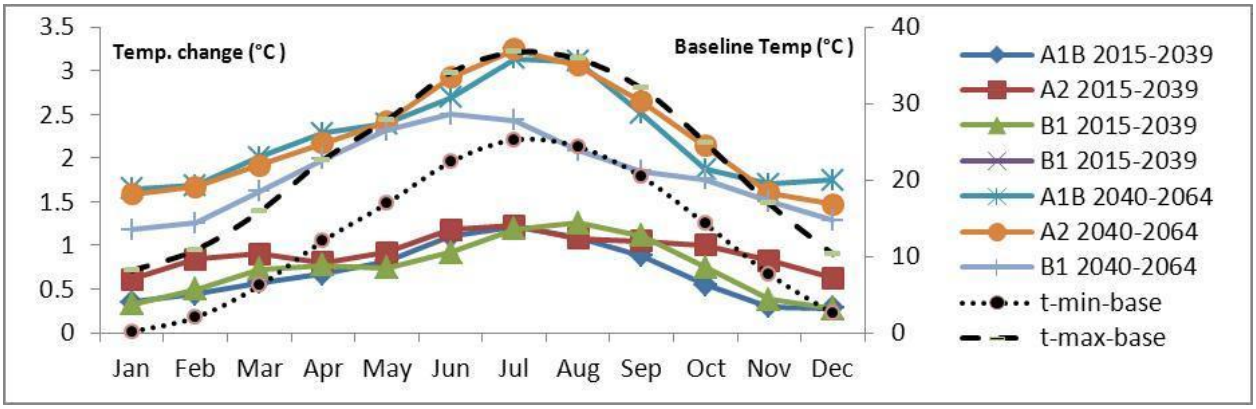

Preprints (www.preprints.org) | NOT PEER-REVIEWED | Posted: 6 September 2022 doi:10.20944/preprints202209.0072.v1



Figure 1. The HadCM3 projected changes in T-min and T-max for Tehran for the short term (2015–2039) and mid-term (2040–2064) periods with respect to the baseline (1972–2009).

HadCM3 projections indicate that the monthly mean surface temperatures are expected to increase under climate change in the study area. Projections show higher average surface temperatures for all months of the year, but the increase is not uniform throughout the year. Temperature rise is projected to be higher in the warm months (JJA), which is an indication of hotter summers in the future. The average surface temperature of the study area is projected to increase by approximately 0.75 °C in short-term and about 2.5 °C in the middle of this century. This temperature rise is expected to exceed 1 °C and 3 °C in the warm month of the year in the short term and mid-term periods, respectively. This trend is noticeable in both short term and mid-term climate periods. In the mid-term period changes in the projections become more distinctive among emission scenarios. Projected changes under A2 and then A1B emission scenarios are expected to be greater than changes under B1 scenario especially in summers where the difference is about 0.5 °C.

Figure 2 shows the projected relative changes in precipitation and radiation for the 2015–2039 and 2040–2064 climate periods with respect to the baseline period under the three emission scenarios at Dushan Tappeh station. Projections illustrate explicit reverse variations in annual patterns of precipitation and radiation under climate change in the future. Projections show that precipitation will decrease in springs and summers, while it will increase in falls and winters with respect to its baseline values. Radiation, in contrast to the precipitation, is projected to increase in springs and summers, and decrease in falls and winters with respect to its baseline values. The results suggest that maximum decrease in precipitation is expected in summers, about 15% and 30% with respect to the baseline period in short term and mid-term respectively. Unlike the precipitation, the greatest increase in solar radiation is projected in summers, about 1% and 2% in short term and mid-term respectively. These reverse patterns suggest that the decrease in precipitation and cloud cover in summers affects the amount of solar radiation received by the earth surface in the study area. Climate simulations for future periods over the study area exhibit behaviors favorable to surface O3 formation. In general, HadCM3 GCM model projections show an increase in temperature with the greatest changes in summers under all three emission scenarios. Moreover, solar radiation is projected to increase in summers in all simulations, due to the decreases in precipitation and cloud cover over the study area. These patterns expect to influence O3 production over the study area in the future.

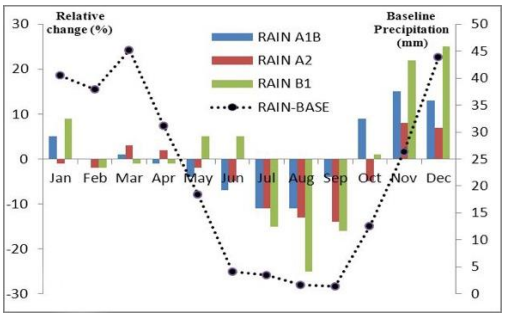


(a)

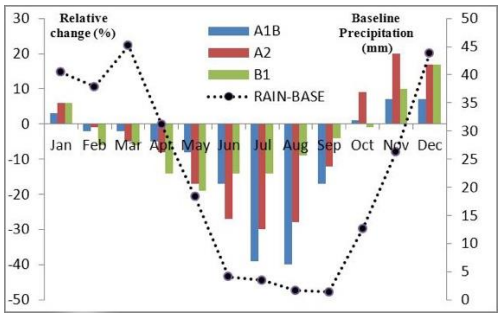


(b)

Preprints (www.preprints.org) | NOT PEER-REVIEWED | Posted: 6 September 2022 doi:10.20944/preprints202209.0072.v1



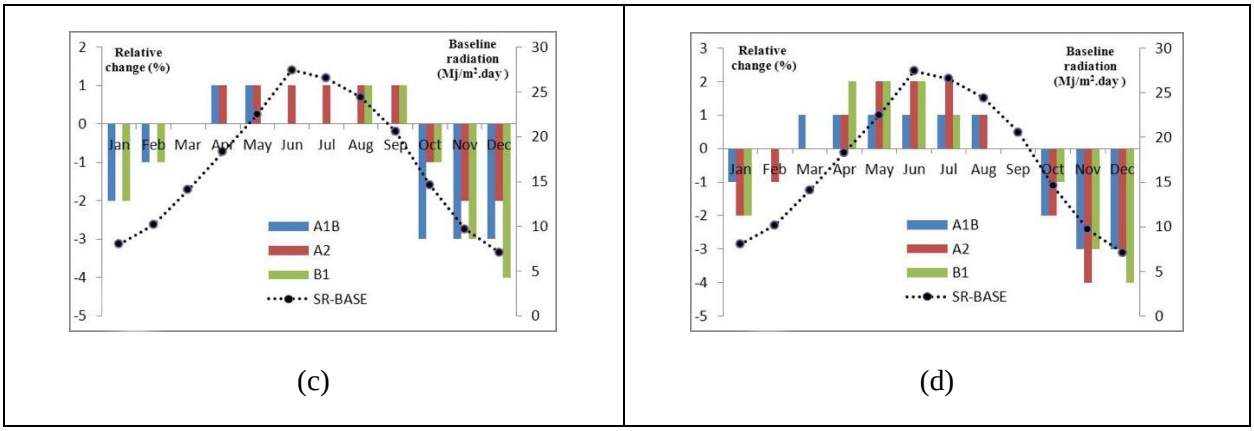


Figure 2. The projected relative changes in precipitation (a and b) and solar radiation (c and d) at Dushan Tappeh station for the short term (2015–2039) (left panel) and mid-term (2040–2064) (right panel).

*3.3. Statistics of air quality levels in the study area*

Figure 3 illustrates the observed monthly means of the air quality variables used in this study that are averaged over the 2009–2012 period. The mean monthly variations of temperature (T) and solar radiation (SR) indicate that the solar radiation in June, and after a month delay, the temperature in July reach their highest values. Therefore, having the highest temperatures and relatively the highest radiation, June, July and August were considered as the warm months of the study area.

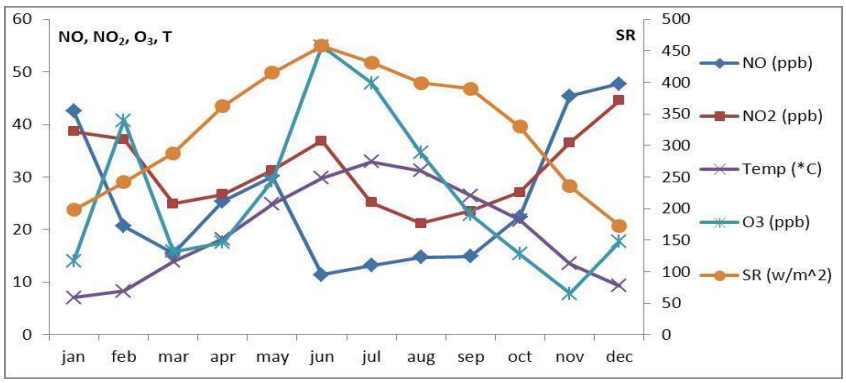


Figure 3. Mean annual cycles of NO, NO2, O3, SR and T at the Golbarg air quality monitoring station for the period 2009–2012.

Moreover, Figure 3 indicates that the observed monthly mean O3 concentrations at the Golbarg air quality station have their highest values in the warm months of JJA. O3 production in the atmosphere is highly dependent on high temperature which usually occur in the warm months with abundant solar radiation. Also, considering the climate projections over the study area indicate that temperature and radiation will be higher in the warm months in the future, we decided to limit the evaluation of climate change impacts on future O3 concentrations to only the warm months in the study area, i.e., JJA.

Figure 4 clearly shows the difference between the pollution conditions in the two summers of 2010 (a) and 2012 (b) in the context of the mean diurnal variations of the variables in the JJA of at the Golbarg air quality station. Among the four summers of 2009 to 2012, summers of 2010 and 2012 had the most and the least number of days with exceedance of O3 air quality standards, respectively. The number of exceedance days was much higher in 2010 than in 2012 due to the more favorable meteorological conditions in the summer of 2010. In the summer of 2010 and in terms of one-hour (1-hr) O3 standard, total of 22 days and in terms of eight-hour (8-hr) O3 standard, total of 58 days exceeded the 120

Preprints (www.preprints.org) | NOT PEER-REVIEWED | Posted: 6 September 2022 doi:10.20944/preprints202209.0072.v1



and 75 ppb concentration threshold respectively. However, in the summer of 2012 no polluted day was occurred in terms of any O3 air quality standard. Table 2 also shows the statistical characteristics of the variables for the two summers. Summer of 2010 experienced higher O3 concentrations in JJAs compared to the summer of 2012 in terms of both seasonal means and mean diurnal concentrations.

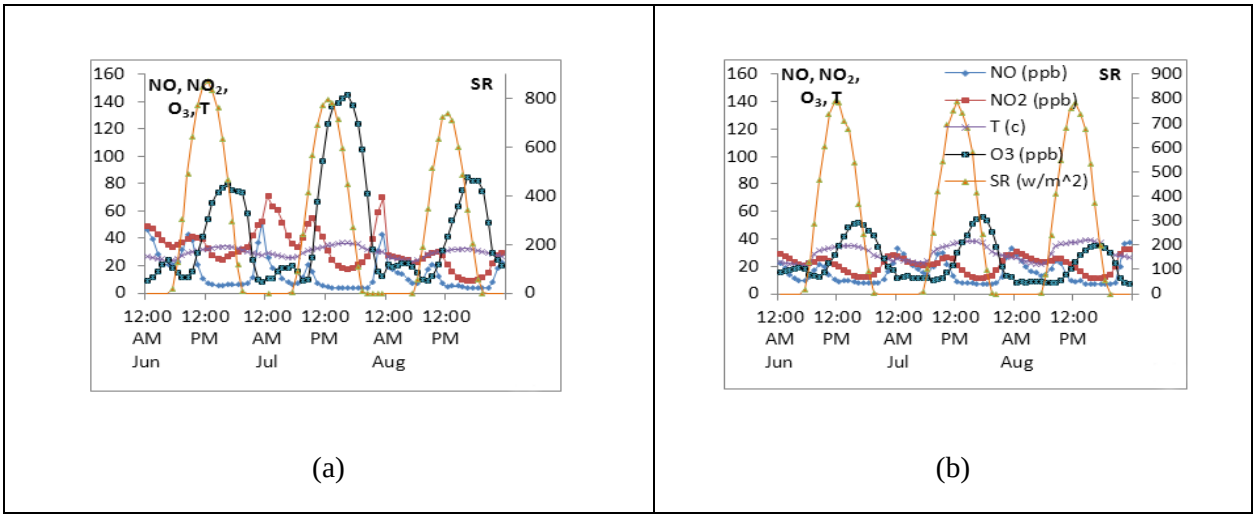


Figure 4. Mean diurnal cycles of NO, NO2, O3, SR and T at the Golbarg air quality monitoring station for the summers of 2010 (a) and 2012 (b).

**Table 2.** Statistical review of the pollution and meteorological variables for the summers of 2010 and 2012.

| Summer 2010 | Variables | Minimum | Maximum | Average | Standard deviation |
|---|---|---|---|---|---|
| | NO (ppb) | 3.5 | 106 | 9.3 | 13.9 |
| | NO2 (ppb) | 4 | 149 | 26.6 | 17 |
| | O3 (ppb) | 4 | 280.4 | 71.2 | 51.8 |
| | T (C) | 23.58 | 42.67 | 32.6 | 3.1 |
| | SR (w/m2) | 0 | 939 | 506.1 | 270.3 |
| Summer 2012 | Variables | Minimum | Maximum | Average | Standard deviation |
| | NO (ppb) | 6.5 | 82.14 | 11.7 | 9.8 |
| | NO2 (ppb) | 7.2 | 50.17 | 17.5 | 7.26 |
| | O3 (ppb) | 6.5 | 96.53 | 33.45 | 17.56 |
| | T (C) | 20.54 | 43.1 | 35 | 3.66 |
| | SR (w/m2) | 0 | 902 | 493 | 272.3 |

*3.4. Development and validation of the AQFM*

To find the optimal architecture for the AQFM, several structures with different numbers of hidden layers and nodes were evaluated. Two out of several various examined architectures with the calculated statistical parameters from the test data sets are shown in Table 3. Statistical parameters indicate that the network with two hidden layers, which has higher correlation coefficient (R) and lower MBE, MAE and RMSE, can better capture the complex and nonlinear relationships among variables of the model. Consequently, the architecture with two hidden layers was selected for the AQFM.

**Table 3.** Calculated statistical parameters for the two developed models.

Preprints (www.preprints.org) | NOT PEER-REVIEWED | Posted: 6 September 2022 doi:10.20944/preprints202209.0072.v1



| | No. of neurons | R | MBE | MAE | RMSE |
|---|---|---|---|---|---|
| 1 hidden layer | 10 | 0.82 | -1.77 | 14.5 | 21.38 |
| 2 hidden layers | 10 | 0.84 | -0.9 | 13.8 | 20.43 |

The correlation between the simulated (horizontal axis) and observed O3 concentrations (vertical axis) for the test data sets of the model are shown in Figure 5. The correlation coefficient is about 0.84 which indicates an acceptable agreement between observed and simulated O3 concentrations at the Golbarg air quality monitoring station. The MBE index is about $-0.9$ ppb. The negative value indicates that the forecast model underestimates the hourly O3 concentrations about 0.9 ppb under the actual observed values. This can be due to the absence of VOC concentrations in the simulation process (Liu et al., 1987). The evaluation criteria of the forecast model are in the acceptable range compared to other similar studies (Arhami et al., 2013; Comrie, 1997; Sousa et al., 2007). In comparison with similar studies, the MAE and RMSE, about 13.8 and 20.43 ppb respectively, are also in the acceptable range which indicate the acceptable performance of the AQFM in predicting hourly O3 concentrations with the least number of input variables.

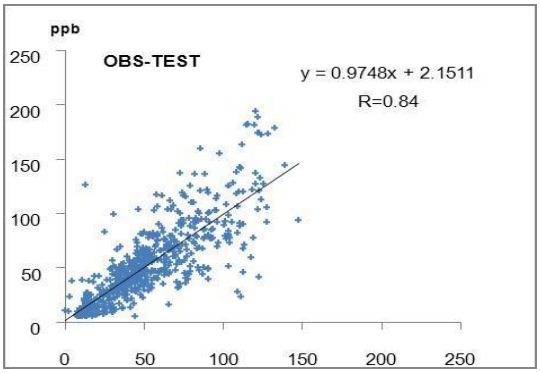


**Figure 5.** Simulated vs. observed O3 concentrations.

Table 4 shows the ability of the AQFM to capture the exceedances of selected concentration thresholds with their corresponding references. As this table indicates, the developed model gives an acceptable prediction performance compared to the similar study (Nunnari et al., 1998). In detecting exceedances of 25 ppb and 45 ppb thresholds, the model can identify 95.7% and 85.9% of exceedances with the overestimation error of 19% and 15.7% respectively. Moreover, in higher concentrations (exceedances of 120 ppb) the developed model can detect about 40% of exceedances with the overestimation error of about 1%. Therefore, regarding the high concentration thresholds and also the number of the model inputs, the AQFM represents a relatively acceptable performance in predicting the violations.

**Table 4.** Performance of the forecast model at selected concentration thresholds with their corresponding references (Results from a similar study are shown in parentheses).

| Reference | Time period | O3 threshold (ppb) | PI 1 (%) | PI 2 (%) |
|---|---|---|---|---|
| O3 Standard | 1 hr | 125 | 13.8 | 0.48 |
| O3 AQI | 1 hr | 120 | 39.4 | 0.9 |
| O3 Information Level (EPA) | 1 hr | 90 | 54.5 | 5.4 |
| Nunnari et al. (1998) | 1 hr | 45 | 85.9 (64.57) | 15.7 (4.25) |

 doi:10.20944/preprints202209.0072.v1



| | | |
|---|---|---|
| 25 | 95.7 (97.75) | 19 (18.03) |

*3.5. Extracting necessary parameters for future diurnal patterns of temperature and radiation*

In methodology section some equations were developed to estimate the diurnal distribution of temperature in the study area. In order to develop these sets of equations, $DL$, $LSH$ and $P$ parameters were needed. We extracted these parameters from Figure 4 at the *Golbarg* air quality station. $LSH$, the maximum solar height, was set to 12 according to Figure 4. The time lag between the occurrence of maximum temperature and maximum solar height in a day, $P$, was set to 3.5 hours according to Figure 4. The day length, $DL$, was obtained from US Navy website (http://www.us.navy.com) according to the location of the station and the study period. To obtain hourly temperature values during a day, the parameters were replaced in the developed temperature equations. Then, the downscaled minimum and maximum temperatures from LARS-WG for each day were replaced in the equations and hourly temperatures were obtained for each day. Solar radiation output from LARS-WG represents daily total radiation received by the earth surface in $Mj/m^2.day$. Downscaled radiation values were distributed during the day according to discussed approach in methodology to obtain hourly values in $w/m^2$. In these sets of equations, $LSH$ was considered 12 for the Golbarg air quality station in the study area.

*3.6. Climate change impacts on Ozone air quality*

In this study, we investigated the impact of climate change on future O3 concentrations. We investigated A1B (moderate), A2 (warm) and B1 (cool) SRES emission scenarios, and summers of 2010 and 2012 as two pollution scenarios. The pollution scenarios were considered constant based on current conditions and therefore only the impact of climate change on future O3 air quality was investigated by assuming that NO and NO2 levels stay constant based on hourly monitored concentrations in the summers of 2010 and 2012. Finally, six different input scenarios to the AQFM were obtained and analyzed for the climate periods of 2015–2039 (short term) and 2040–2064 (mid-term).

3.6.1. Projected trends in future ozone exceedance days

The USEPA considers the 120 and 75 ppb O3 concentrations as the thresholds for violating 1-hr and 8-hr O3 air quality standards, respectively. In this study, we used the number of days that hourly O3 concentrations exceeded each of these thresholds, so multiple exceedances within a single day were not counted for the study area.

Figure 6a compares the changes in the number of days that exceed 1-hr O3 standard in on both present pollution conditions (2010 and 2012). In the summer of 2010, 22 days exceeded 1-hr O3 standard and no exceedances were occurred in the summer of 2012. The projections indicate that the number of polluted days will increase under future climate in both emission scenarios. The number of polluted days in terms of the number of exceedances from 1-hr standard is projected to grow even based on violation-free summer of 2012. Figure 6b compares the changes in the number of days that exceed 8-hr O3 standard in both emission scenarios as a result of changes in future climate. Similar to 1-hr exceedances (Figure 6a), the projections show an increase in the number of 8-hr exceedances under the future climate by assuming no changes in the present pollution conditions. Although the summer of 2010 was a highly polluted summer, climate change still has an increasing influence on the number of projected polluted days. In the mid-term, due to projected higher O3 concentrations, exceedances of 8-hr standard will increase and the controlling standard will shift from 1-hr to 8-hr standard.

Preprints (www.preprints.org) | NOT PEER-REVIEWED | Posted: 6 September 2022 doi:10.20944/preprints202209.0072.v1



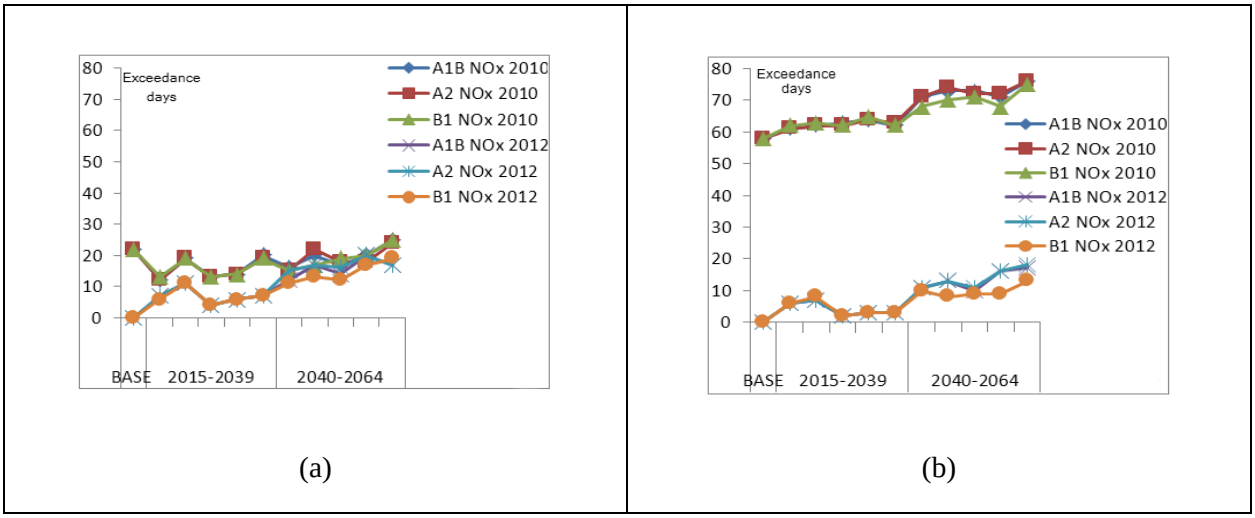


Figure 6. Projected days per summer (JJA) with exceedances of 1-hr (a) and 8-hr (b) O3 standard based on summers of 2010 and 2012 scenarios.

Regardless of existing uncertainties in different parts of the climate change impact assessment such as uncertainties in climate sensitivity and future greenhouse gasses emission pathways, projections indicate that because of occurring more favorable O3 formation conditions in the future due to climate change, the number of O3 polluted days will increase over all emission scenarios and climate periods, even based on the violation-free pollution scenario of the summer of 2012. Summer of 2010 was a year with the highest monitored O3 concentrations in the observations probably due to meteorological conditions favorable to O3 formation. About 58 out of 92 days of the 2010 summer violated 8-hr O3 standard while 2012 experienced a violation-free summer. These 2 scenarios can serve as a suitable example for analyzing the sensitivity of O3 air quality under future climate changes while emissions are held constant over future decades.

Furthermore, comparing changes in the projected O3 exceedances in the two climate periods, short term changes based on each pollution scenarios are almost overlapped, and no noticeable distinction exists between different emission scenarios. However, due to the inertia in the climate system, inter-scenario differences among SRES emission scenarios will emerge after 2030 and the differences between projections are more pronounced in mid-term and long-term projections (Stott and Kettleborough, 2002).

3.6.2. Projected average number of ozone polluted days in each climate period

Due to the stochastic nature of the downscaling techniques, it is more reasonable to consider only the changes in the number of exceedances in each climate period instead of a specific year in the future. Figure 7 illustrates the projected average number of exceedances of 8-hr O3 standard in each climate period for each emission scenario. The number of polluted days in both emission scenarios rises in the future. In the short term, the largest increase in the number of polluted days is anticipated for the B1 emission scenario and in the mid-term the largest increase is projected for the A2 simulations. In the short term and based on summer of 2010 scenario, the largest increase is expected to be about 8.3% for the B1 scenario from 58 exceedance days in 2010 to 62.8 exceedance days in the short term. In the mid-term, the largest increase is expected to be about 26% for the A2 scenario from 58 exceedance days in 2010 to 73 exceedance days in the mid-term. Likewise, based on summer of 2012 scenario, all scenarios show an increase in the number of exceedance days. In the short term, the largest increase in the number of exceedance days is anticipated for the B1 scenario and this number grows from zero in 2012 to 4.4 days in the short

Preprints (www.preprints.org) | NOT PEER-REVIEWED | Posted: 6 September 2022 doi:10.20944/preprints202209.0072.v1



term. In the mid-term, the largest increase in the number of exceedance days is projected for the A2 scenario and this number grows from zero in 2012 to 13.8 days in the mid-term.

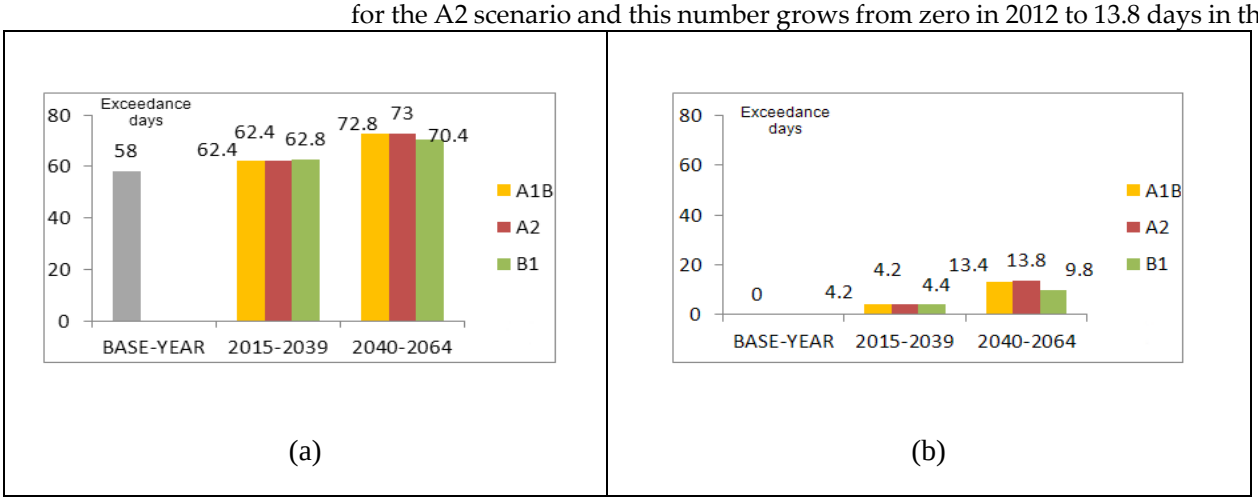


Figure 7. Projected average number of summer days (JJA) with exceedance of 8-hr O3 standard based on summers of 2010 (a) and 2012 (b).

3.6.3. Projected trends in future ozone Air Quality Index exceedances (AQI)

The projected O3 concentrations were also analyzed from health-related metrics such as 1-hr and 8-hr O3 Air Quality Indices (AQI). In this section only the 8-hr projections for the A1B emission scenario are presented. Figure 8 shows the change in the number of days with exceedance of the 8-hr O3 AQI concentration thresholds under the A1B emission scenario for summers of 2010 (a) and 2012 (b). Projections indicate an increase in the number of O3 *Unhealthy* and *Very Unhealthy* days under the impact of climate change which reflects the degradation of O3 air quality in the future.

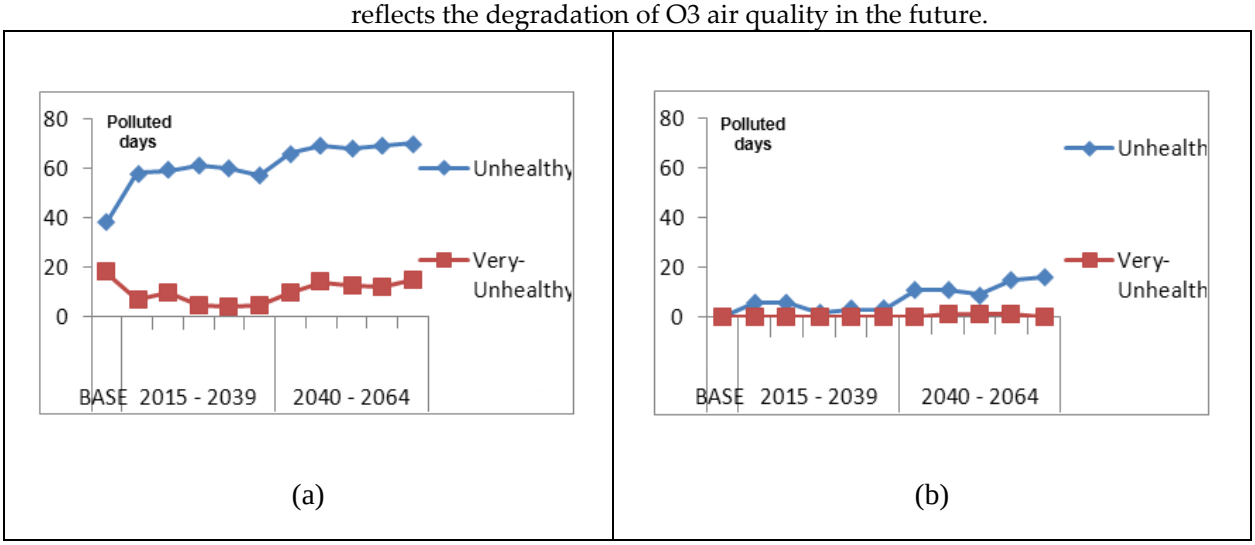


Figure 8. Projected days per summer (JJA) with exceedances of 8-hr O3 AQI based on summers of 2010 (a) and 2012 (b).

Figure 8a shows that based on summer of 2010 scenario, the number of *Unhealthy* days increases over both climate periods, while the number of *Very Unhealthy* days decreases over the first period and then increases in the second period. Figure 8b shows that based on the summer of 2010 scenario, the number of *Unhealthy* days grows over the two future climate periods. Occurrence of the *Very Unhealthy* days are not expected over the first climate period, but due to the projected higher temperature and radiation, the number of the *Very Unhealthy* days starts to grow over the second climate period.

Preprints (www.preprints.org) | NOT PEER-REVIEWED | Posted: 6 September 2022 doi:10.20944/preprints202209.0072.v1



The average number of polluted days was calculated for each climate period. In this section only the projections for the 8-hr O3 AQI under A1B emission scenario are demonstrated. Figure 9 shows the average number of polluted days in the 8-hr O3 AQI for the pollution conditions in the summers of 2010 (a) and 2012 (b). As the Figure 9a shows, the average number of *Unhealthy* days is expected to grow over the two future climate periods. The number of *Unhealthy* days was 38 days in the summer of 2010, which is projected to increase about 55% over the first period, averaging about 59 days in the short term, and about 80% over the second period, averaging about 68.5 days in the mid-term. The number of *Very Unhealthy* days is projected to fall about 65% from 18 days in the summer of 2010 to 6.2 days in the first period, but is projected to double in the second period by increasing from 6.2 days to 12.8 days in the mid-term period.

Figure 9b shows an increase in the average number of polluted days based on the summer of 2012 scenario. No *Unhealthy* day was observed in the summer of 2012. However, projections estimate about 4 *Unhealthy* days without any *Very Unhealthy* days in the short-term period. In the mid-term period, the average number of *Unhealthy* days is expected to increase to 12 days with one Very Unhealthy day.

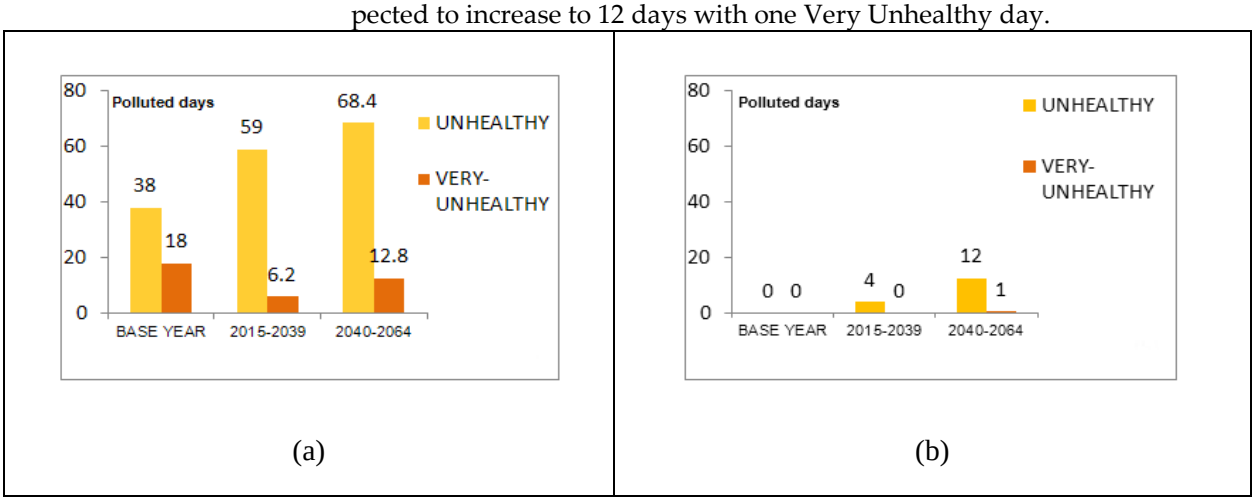


Figure 9. Projected average number of summer days (JJA) with exceedance of 8-hr O3 AQI based on summers of 2010 (a) and 2012 (b).

## 4. Summary and conclusion

In this study, we investigated the impact of climate change on future summertime O3 concentrations in Tehran, Iran. We used three IPCC greenhouse gas emission scenarios to simulate future climate: A1B, A2, and B1, which their emissions are equivalent to RCP4.5, RCP8.5, and RCP2.6, respectively. These climate projections were obtained from HACM3 GCM and were downscaled by the LARS-WG5 model over the periods of 2015–2039 and 2040–2064.

Climate change projections indicate that our study area becomes warmer over the next 50 years. The projected increases in temperature and solar radiation along with the decreases in precipitation and cloud cover for the future summers over the study area are indications of more favorable conditions for photochemical pollution formation which could consequently result in degraded air quality conditions in future summers. To quantify the impact of projected climate change on future O3 levels, we developed a neural network as our AQFM. We used temperature, solar radiation, NO and NO2 as inputs to our AQFM. The projections were performed by assuming that current emission conditions of O3 precursors remain constant in the future. Therefore, pollution conditions of the summers of 2010 and 2012 were considered as two different pollution scenarios and only the impact of climate change alone were accounted in the projections. The simulations project that the number of O3 polluted days would increase based on both summer emission sce-

narios. The increase based on the exceedance-free summer of 2012 would be more noticeable compared to the highly polluted summer of 2010. Moreover, the growing number of polluted days in terms of 8-hr indices compared to 1-hr indices could be an indication of more exposure to higher O3 concentrations in the future.

Since this study is considered as one of the first studies in Iran which addresses the influence of future climate on air quality, it was subject to various limitations. One of the major limitations was that NMVOC concentrations were not included in the simulations due to unavailability of this data. O3 simulations without considering NMVOCs in the calculation process tend to underestimate O3 concentrations (Liu et al., 1987). O3 production is sensitive to other climate variables such as wind speed, water vapor, cloud cover or precipitation (Dawson et al., 2007). However, due to simplification in the modeling process, only temperature and solar radiation were selected in this study. Another limitation in this study is the assumption that emissions of O3 precursors and their relationship with O3 formation remain constant in the future and therefore the role of future emission reductions cannot be considered in the simulations. To reduce the scope of this limitation in our simulations, two different summertime pollution conditions with the highest and the lowest number of monitored polluted days were considered in this modeling endeavor to demonstrate the probable range of future changes in O3 pollution.

Future research should therefore consider the limitations in this study. Since the absence of NMVOC concentrations as one of the main precursors of O3 production reduces the accuracy in the simulations, future studies could benefit from including NMVOC concentrations in simulations. Moreover, regarding existing uncertainties in GCM projections, future studies should also consider ensemble projection approaches by incorporating several GCMs in climate change impact assessments to improve the level of confidence in air quality projections. Furthermore, using dynamical downscaling results from Regional Climate Models, including other climate variables in projections, and comparing projections of statistical approaches with projections of Chemistry Transport Models could be other useful measures to consider for improving the accuracy and confidence in the climate change impact assessments.

## References


1. Alibak, A.H., Khodarahmi, M., Fayyazsanavi, P., Alizadeh, S.M., Hadi, A.J., Aminzadehsarikhanbeglou, E., 2022. Simulation the adsorption capacity of polyvinyl alcohol/carboxymethyl cellulose based hydrogels towards methylene blue in aqueous solutions using cascade correlation neural network (CCNN) technique. J. Clean. Prod. 337, 130509. https://doi.org/10.1016/j.jclepro.2022.130509
2. Arhami, M., Kamali, N., Rajabi, M.M., 2013. Predicting hourly air pollutant levels using artificial neural networks coupled with uncertainty analysis by Monte Carlo simulations. Environ. Sci. Pollut. Res. 20, 4777–4789. https://doi.org/10.1007/s11356-012-1451-6
3. Ashrafi, K., 2012. Determining of spatial distribution patterns and temporal trends of an air pollutant using proper orthogonal decomposition basis functions. Atmos. Environ. 47, 468–476. https://doi.org/10.1016/j.atmosenv.2011.10.016
4. Atash, F., 2007. The deterioration of urban environments in developing countries: Mitigating the air pollution crisis in Tehran, Iran. Cities 24, 399–409. https://doi.org/10.1016/j.cities.2007.04.001
5. Baertsch-Ritter, N., Keller, J., Dommen, J., Prevot, A.S.H., 2004. Effects of various meteorological conditions and spatial emissionresolutions on the ozone concentration and ROG/$NO_x$ limitationin the Milan area (I). Atmospheric Chem. Phys. 4, 423–438. https://doi.org/10.5194/acp-4-423-2004
6. Beale, M.H., Hagan, M.T., Demuth, H.B., 2012. Neural Network Toolbox™ User's Guide, in: R2012a, The MathWorks, Inc., 3 Apple Hill Drive Natick, MA 01760-2098, , Www.Mathworks.Com.
7. Bell, M.L., Goldberg, R., Hogrefe, C., Kinney, P.L., Knowlton, K., Lynn, B., Rosenthal, J., Rosenzweig, C., Patz, J.A., 2007. Climate change, ambient ozone, and health in 50 US cities. Clim. Change 82, 61–76. https://doi.org/10.1007/s10584-006-9166-7
8. Camalier, L., Cox, W., Dolwick, P., 2007. The effects of meteorology on ozone in urban areas and their use in assessing ozone trends. Atmos. Environ. 41, 7127–7137. https://doi.org/10.1016/j.atmosenv.2007.04.061
9. Chaloulakou, A., Saisana, M., Spyrellis, N., 2003. Comparative assessment of neural networks and regression models for forecasting summertime ozone in Athens. Sci. Total Environ. 313, 1–13. https://doi.org/10.1016/S0048-9697(03)00335-8
10. Comrie, A.C., 1997. Comparing Neural Networks and Regression Models for Ozone Forecasting. J. Air Waste Manag. Assoc. 47, 653–663. https://doi.org/10.1080/10473289.1997.10463925

11. Cox, W.M., Chu, S.-H., 1996. Assessment of interannual ozone variation in urban areas from a climatological perspective. Atmos. Environ. 30, 2615–2625. https://doi.org/10.1016/1352-2310(95)00346-0
12. Dawson, J.P., Adams, P.J., Pandis, S.N., 2007. Sensitivity of ozone to summertime climate in the eastern USA: A modeling case study. Atmos. Environ. 41, 1494–1511. https://doi.org/10.1016/j.atmosenv.2006.10.033
13. Dawson, J.P., Racherla, P.N., Lynn, B.H., Adams, P.J., Pandis, S.N., 2009. Impacts of climate change on regional and urban air quality in the eastern United States: Role of meteorology. J. Geophys. Res. Atmospheres 114. https://doi.org/10.1029/2008JD009849
14. Ebi, K.L., McGregor, G., 2008. Climate Change, Tropospheric Ozone and Particulate Matter, and Health Impacts. Environ. Health Perspect. 116, 1449–1455. https://doi.org/10.1289/ehp.11463
15. Ephrath, J.E., Goudriaan, J., Marani, A., 1996. Modelling diurnal patterns of air temperature, radiation wind speed and relative humidity by equations from daily characteristics. Agric. Syst. 51, 377–393. https://doi.org/10.1016/0308-521X(95)00068-G
16. Fuentes, J.D., Lerdau, M., Atkinson, R., Baldocchi, D., Bottenheim, J.W., Ciccioli, P., Lamb, B., Geron, C., Gu, L., Guenther, A., Sharkey, T.D., Stockwell, W., 2000. Biogenic Hydrocarbons in the Atmospheric Boundary Layer: A Review. Bull. Am. Meteorol. Soc. 81, 1537–1575.
17. Gardner, M.W., Dorling, S.R., 1998. Artificial neural networks (the multilayer perceptron)—a review of applications in the atmospheric sciences. Atmos. Environ. 32, 2627–2636. https://doi.org/10.1016/S1352-2310(97)00447-0
18. Gryparis, A., Forsberg, B., Katsouyanni, K., Analitis, A., Touloumi, G., Schwartz, J., Samoli, E., Medina, S., Anderson, H.R., Niciu, E.M., Wichmann, H.-E., Kriz, B., Kosnik, M., Skorkovsky, J., Vonk, J.M., Dörtbudak, Z., 2004. Acute Effects of Ozone on Mortality from the "Air Pollution and Health. Am. J. Respir. Crit. Care Med. 170, 1080–1087. https://doi.org/10.1164/rccm.200403-333OC
19. Guenther, A., Geron, C., Pierce, T., Lamb, B., Harley, P., Fall, R., 2000. Natural emissions of non-methane volatile organic compounds, carbon monoxide, and oxides of nitrogen from North America. Atmos. Environ. 34, 2205–2230. https://doi.org/10.1016/S1352-2310(99)00465-3
20. Halek, F., Kavouci, A., Montehaie, H., 2004. Role of motor-vehicles and trend of air borne particulate in the Great Tehran area, Iran. Int. J. Environ. Health Res. 14, 307–313. https://doi.org/10.1080/09603120410001725649
21. Hessami, M., Gachon, P., Ouarda, T.B.M.J., St-Hilaire, A., 2008. Automated regression-based statistical downscaling tool. Environ. Model. Softw. 23, 813–834. https://doi.org/10.1016/j.envsoft.2007.10.004
22. Holloway, T., Spak, S.N., Barker, D., Bretl, M., Moberg, C., Hayhoe, K., Van Dorn, J., Wuebbles, D., 2008. Change in ozone air pollution over Chicago associated with global climate change. J. Geophys. Res. Atmospheres 113. https://doi.org/10.1029/2007JD009775
23. Hosseinpoor, A.R., Forouzanfar, M.H., Yunesian, M., Asghari, F., Naieni, K.H., Farhood, D., 2005. Air pollution and hospitalization due to angina pectoris in Tehran, Iran: A time-series study. Environ. Res. 99, 126–131. https://doi.org/10.1016/j.envres.2004.12.004
24. Hoveidi, H., Aslemand, A., Vahidi, H., Akhavan, F., 2013. Cost Emission of Pm10 on Human Health Due to the Solid Waste Disposal Scenarios, Case Study; Tehran, Iran. J. Earth Sci. Clim. Change. https://doi.org/10.4172/2157-7617.1000139
25. IPCC, 2007: Summary for Policymakers. In: Climate Change 2007: The Physical Science Basis. Contribution of Working Group I to the Fourth Assessment Report of the Intergovernmental Panel on Climate Change [Solomon, S., D. Qin, M. Manning, Z. Chen, M. Marquis, K.B. Averyt, M.Tignor and H.L. Miller (eds.)]. Cambridge University Press, Cambridge, United Kingdom and New York, NY, USA.
26. IPCC, 2021: Summary for Policymakers. In: Climate Change 2021: The Physical Science Basis. Contribution of Working Group I to the Sixth Assessment Report of the Intergovernmental Panel on Climate Change [Masson-Delmotte, V., P. Zhai, A. Pirani, S.L. Connors, C. Péan, S. Berger, N. Caud, Y. Chen, L. Goldfarb, M.I. Gomis, M. Huang, K. Leitzell, E. Lonnoy, J.B.R. Matthews, T.K. Maycock, T. Waterfield, O. Yelekçi, R. Yu, and B. Zhou (eds.)]. Cambridge University Press, Cambridge, United Kingdom and New York, NY, USA, pp. 3–32, doi:10.1017/9781009157896.001.
27. Jacob, D.J., Winner, D.A., 2009. Effect of climate change on air quality. Atmos. Environ., Atmospheric Environment - Fifty Years of Endeavour 43, 51–63. https://doi.org/10.1016/j.atmosenv.2008.09.051
28. Jacobson, M.Z., 2005. Fundamentals of Atmospheric Modeling, 2nd ed. Cambridge University Press, Cambridge. https://doi.org/10.1017/CBO9781139165389
29. Lee, B.-S., Wang, J.-L., 2006. Concentration variation of isoprene and its implications for peak ozone concentration. Atmos. Environ. 40, 5486–5495. https://doi.org/10.1016/j.atmosenv.2006.03.035
30. Leibensperger, E.M., Mickley, L.J., Jacob, D.J., 2008. Sensitivity of US air quality to mid-latitude cyclone frequency and implications of 1980–2006 climate change. Atmospheric Chem. Phys. 8, 7075–7086. https://doi.org/10.5194/acp-8-7075-2008
31. Liao, H., Chen, W.-T., Seinfeld, J.H., 2006. Role of climate change in global predictions of future tropospheric ozone and aerosols. J. Geophys. Res. Atmospheres 111. https://doi.org/10.1029/2005JD006852
32. Lioubimtseva, E., Henebry, G.M., 2009. Climate and environmental change in arid Central Asia: Impacts, vulnerability, and adaptations. J. Arid Environ. 73, 963–977. https://doi.org/10.1016/j.jaridenv.2009.04.022

33. Liu, S.C., Trainer, M., Fehsenfeld, F.C., Parrish, D.D., Williams, E.J., Fahey, D.W., Hübler, G., Murphy, P.C., 1987. Ozone production in the rural troposphere and the implications for regional and global ozone distributions. J. Geophys. Res. Atmospheres 92, 4191–4207. https://doi.org/10.1029/JD092iD04p04191
34. Lynn, B.H., Druyan, L., Hogrefe, C., Dudhia, J., Rosenzweig, C., Goldberg, R., Rind, D., Healy, R., Rosenthal, J., Kinney, P., 2004. Sensitivity of present and future surface temperatures to precipitation characteristics. Clim. Res. 28, 53–65. https://doi.org/10.3354/cr028053
35. Mejia, J., Wilcox, E., Rayne, S., Mosadegh, E., 2018. Final report: Vehicle Miles Traveled Review. https://doi.org/10.13140/RG.2.2.29814.52807
36. Millstein, D.E., Harley, R.A., 2009. Impact of climate change on photochemical air pollution in Southern California. Atmospheric Chem. Phys. 9, 3745–3754. https://doi.org/10.5194/acp-9-3745-2009
37. Mosadegh, E., 2013. Modeling the Regional Effects of Climate Change on Future Urban Air Quality (With Special Reference to Future Ozone Concentrations in Tehran, Iran). Univ. Tehran, Iran. DOI: 10.13140/RG.2.2.23815.32165
38. Mosadegh, E., Babaeian, I., 2022a. Projection of Temperature and Precipitation for 2020-2100 Using Post-processing of General Circulation Models Output and Artificial Neural Network Approach, Case Study: Tehran and Alborz Provinces. Iranian Journal of Geophysics. https://doi.org/10.30499/ijg.2022.311104.1370
39. Mosadegh, E., Babaeian, I., 2022b. Quantifying the Range of Uncertainty in GCM Projections for Future Solar Radiation, Temperature and Precipitation under Global Warming Effect in Dushan-Tappeh Station, Tehran, Iran. Iranian Journal of Geophysics. https://doi.org/10.30499/ijg.2022.310958.1369
40. Mosadegh, E., Mejia, J., Wilcox, E.M., Rayne, S., 2018. Vehicle Miles Travel (VMT) trends over Lake Tahoe area and its effect on Nitrogen Deposition 2018, A23M-3068.
41. Mosadegh, E., Nolin, A.W., 2020. Estimating Arctic sea ice surface roughness by using back propagation neural network 2020, C014-0005.
42. Mott, J.A., Mannino, D.M., Alverson, C.J., Kiyu, A., Hashim, J., Lee, T., Falter, K., Redd, S.C., 2005. Cardiorespiratory hospitalizations associated with smoke exposure during the 1997, Southeast Asian forest fires. Int. J. Hyg. Environ. Health 208, 75–85. https://doi.org/10.1016/j.ijheh.2005.01.018
43. Murazaki, K., Hess, P., 2006. How does climate change contribute to surface ozone change over the United States? J. Geophys. Res. Atmospheres 111. https://doi.org/10.1029/2005JD005873
44. Narumi, D., Kondo, A., Shimoda, Y., 2009. The effect of the increase in urban temperature on the concentration of photochemical oxidants. Atmos. Environ. 43, 2348–2359. https://doi.org/10.1016/j.atmosenv.2009.01.028
45. Nejatishahidin, N., Fayyazsanavi, P., Kosecka, J., 2022. Object Pose Estimation using Mid-level Visual Representations (No. arXiv:2203.01449). arXiv. https://doi.org/10.48550/arXiv.2203.01449
46. Niska, H., Hiltunen, T., Karppinen, A., Ruuskanen, J., Kolehmainen, M., 2004. Evolving the neural network model for forecasting air pollution time series. Eng. Appl. Artif. Intell., Intelligent Control and Signal Processing 17, 159–167. https://doi.org/10.1016/j.engappai.2004.02.002
47. Nunnari, G., Nucifora, A.F.M., Randieri, C., 1998. The application of neural techniques to the modelling of time-series of atmospheric pollution data. Ecol. Model. 111, 187–205. https://doi.org/10.1016/S0304-3800(98)00118-5
48. Ordóñez, C., Mathis, H., Furger, M., Henne, S., Hüglin, C., Staehelin, J., Prévôt, A.S.H., 2005. Changes of daily surface ozone maxima in Switzerland in all seasons from 1992 to 2002 and discussion of summer 2003. Atmospheric Chem. Phys. 5, 1187–1203. https://doi.org/10.5194/acp-5-1187-2005
49. Orru, H., Andersson, C., Ebi, K.L., Langner, J., Åström, C., Forsberg, B., 2013. Impact of climate change on ozone-related mortality and morbidity in Europe. Eur. Respir. J. 41, 285–294. https://doi.org/10.1183/09031936.00210411
50. Racherla, P.N., Adams, P.J., 2006. Sensitivity of global tropospheric ozone and fine particulate matter concentrations to climate change. J. Geophys. Res. Atmospheres 111. https://doi.org/10.1029/2005JD006939
51. Rahnama, M., Noury, M., 2008. Developing of Halil River Rainfall-Runoff Model, Using Conjunction of Wavelet Transform and Artificial Neural Networks. Res. J. Environ. Sci. 2, 385–392. https://doi.org/10.3923/rjes.2008.385.392
52. Schlink, U., Dorling, S., Pelikan, E., Nunnari, G., Cawley, G., Junninen, H., Greig, A., Foxall, R., Eben, K., Chatterton, T., Vondracek, J., Richter, M., Dostal, M., Bertucco, L., Kolehmainen, M., Doyle, M., 2003. A rigorous inter-comparison of ground-level ozone predictions. Atmos. Environ. 37, 3237–3253. https://doi.org/10.1016/S1352-2310(03)00330-3
53. Seinfeld, J.H., Pandis, S.N., 2006. Atmospheric chemistry and physics: from air pollution to climate change, 2nd ed. ed. Wiley, Hoboken, N.J.
54. Semenov, M., Barrow, E., 2002. LARS-WG A Stochastic Weather Generator for Use in Climate Impact Studies.
55. Semenov, M., Stratonovitch, P., 2010. Use of multi-model ensembles from global climate models for assessment of climate change impacts. Clim. Res. - Clim. RES 41, 1–14. https://doi.org/10.3354/cr00836
56. Semenov, M.A., 2007. Development of high-resolution UKCIP02-based climate change scenarios in the UK. Agric. For. Meteorol. 144, 127–138. https://doi.org/10.1016/j.agrformet.2007.02.003
57. Sillman, S., 1999. The relation between ozone, NOx and hydrocarbons in urban and polluted rural environments. Atmos. Environ. 33, 1821–1845. https://doi.org/10.1016/S1352-2310(98)00345-8

58. Sillman, S., Samson, P.J., 1995. Impact of temperature on oxidant photochemistry in urban, polluted rural and remote environments. J. Geophys. Res. Atmospheres 100, 11497–11508. https://doi.org/10.1029/94JD02146
59. Sousa, S.I.V., Martins, F.G., Alvim-Ferraz, M.C.M., Pereira, M.C., 2007. Multiple linear regression and artificial neural networks based on principal components to predict ozone concentrations. Environ. Model. Softw. 22, 97–103. https://doi.org/10.1016/j.envsoft.2005.12.002
60. Spitters, C.J.T., Toussaint, H.A.J.M., Goudriaan, J., 1986. Separating the diffuse and direct component of global radiation and its implications for modeling canopy photosynthesis Part I. Components of incoming radiation. Agric. For. Meteorol. 38, 217–229. https://doi.org/10.1016/0168-1923(86)90060-2
61. Steiner, A.L., Tonse, S., Cohen, R.C., Goldstein, A.H., Harley, R.A., 2006. Influence of future climate and emissions on regional air quality in California. J. Geophys. Res. Atmospheres 111. https://doi.org/10.1029/2005JD006935
62. Stott, P.A., Kettleborough, J.A., 2002. Origins and estimates of uncertainty in predictions of twenty-first century temperature rise. Nature 416, 723–726. https://doi.org/10.1038/416723a
63. Varotsos, K.V., Tombrou, M., Giannakopoulos, C., 2013. Statistical estimations of the number of future ozone exceedances due to climate change in Europe. J. Geophys. Res. Atmospheres 118, 6080–6099. https://doi.org/10.1002/jgrd.50451
64. Webster, M.D., Babiker, M., Mayer, M., Reilly, J.M., Harnisch, J., Hyman, R., Sarofim, M.C., Wang, C., 2002. Uncertainty in emissions projections for climate models. Atmos. Environ. 36, 3659–3670. https://doi.org/10.1016/S1352-2310(02)00245-5
65. Wilby, R., Charles, S., Zorita, E., Timbal, B., Whetton, P., Mearns, L., 2004. Guidelines For Use of Climate Scenarios Developed From Statistical Downscaling Methods. Support. Mater. Intergov. Penel Clim. Change.
66. Wilks, D.S., Wilby, R.L., 1999. The weather generation game: a review of stochastic weather models. Prog. Phys. Geogr. Earth Environ. 23, 329–357. https://doi.org/10.1177/030913339902300302
67. Wise, E.K., 2009. Climate-based sensitivity of air quality to climate change scenarios for the southwestern United States. Int. J. Climatol. 29, 87–97. https://doi.org/10.1002/joc.1713
68. https://doi.org/10.1016/j.atmosenv.2005.01.024
69. Zarghami, M., Abdi, A., Babaeian, I., Hassanzadeh, Y., Kanani, R., 2011. Impacts of climate change on runoffs in East Azerbaijan, Iran. Glob. Planet. Change 78, 137–146. https://doi.org/10.1016/j.gloplacha.2011.06.003